The Treatment of Geometrically Small Structures in FDTD by the Modification of Assigned Material Parameters

Chris J. Railton, Dominique L. Paul, Ian J. Craddock, and Geoffrey S. Hilton

***Abstract*—A number of different improvements to the analysis by finite-difference time-domain (FDTD) of small structures, such as wires, strips and slots have been proposed in the literature. One of these methods takes account of the fringing fields associated with metal edges and wires by empirically modifying the assigned material parameters in neighboring cells. In this contribution it is shown that, in many cases, it is possible to derive these modified assigned material parameters (MAMPs) analytically. In this form, the approach provides an alternative, and novel, way of incorporating Static Field Solutions into the FDTD method which has advantages of simplicity and robustness over existing techniques. Results are presented for a number of structures including wire transmission lines and a microstrip patch antenna.**

***Index Terms*—Author, please supply your own keywords or send a blank e-mail to keywords@ieee.org to receive a list of suggested keywords.**

I. Introduction

In [1], it was shown that the effects of field singularities in the region of wires and strips can be accounted for within the finite-difference time-domain (FDTD) method, by altering the permittivities and permeabilities assigned to the neighboring E and H field nodes. The required values for these modified assigned material parameters (MAMPs) were ascertained empirically by performing many FDTD runs on simple example structures. A mapping between the material parameters and the fringing capacitance and inductance was derived which was then used to produce look-up tables for use in the FDTD program. In [2], it was shown that this technique could be effectively applied to more complex structures, such as a microstrip filter, in a way which reduced the dependency of the results on the choice of the mesh. In addition, the use of this technique allowed a coarser mesh to be used with equivalent accuracy. In [3] the same technique was shown to be effective for a waveguide filter containing a complex iris structure.

In this contribution it is shown that the MAMPs can, in many cases, be calculated analytically thus avoiding the necessity of setting up the empirical look-up tables. The method preserves the robustness and simplicity of [1] but with the added advantage of the rigour of an analytical derivation. Whereas previously published ways of introducing Static Field Solutions into FDTD lead to a direct modification of the coefficients of the update equations, the method described herein leads instead to a modification of the physical parameters of the material. The modeled material is, therefore, always a physical one, so that issues of reciprocity, stability and local charge conservation are much more easily addressed.

In Section II, a comparison of the present method with other published algorithms is given and the benefits of the present method are highlighted. In Section III, it is shown how the MAMPs can be calculated for strips and wires and, finally, Section IV provides a comparison of results obtained using the present method with those in the literature for the examples of stripline, wire transmission line, microstrip and a microstrip patch antenna.

In almost all of the examples tried, it was not necessary to make any reduction in the time step below that which would have been chosen for basic FDTD. For the case of very thin wires or very narrow strips the time step did need to be reduced but in no case was it found necessary to reduce the time step below 0.7 of the Courant limit for basic FDTD.

II. Comparison With Previous Work

Much work has been reported in the literature aimed at including the effects of field singularities into the FDTD mesh by altering the update equations appropriately. The philosophy of the majority of these methods can be summarized by considering the example of a wedge placed in the FDTD mesh in such a way that the edge is aligned with the z axis. This is shown in Fig. 1.

The behavior of the fields in the vicinity of the wedge can be expressed as a Laurent series as given in (1) [4]

$$E_z = \sum_k c_k r^{\nu_k} \sin(\nu_k \phi) \tag{1}$$

where $\nu_k = n\pi/(2\pi - \alpha)$, α is the wedge angle and ϕ is the angle between the wedge and the observation point.

In standard FDTD, the update equations for the H_z field component nearest the edge, derived from the integral form of Ampere's Law, is given by

$$\mu \delta x \delta y \frac{\partial H_z}{\partial t} = E_{x,j+1}\delta x + E_{y,i}\delta y - E_{x,j}\delta x - E_{y,i+1}\delta y. \tag{2}$$

This approximation to the integrals assumes that the field amplitudes vary linearly between nodes. In order to incorporate the

Manuscript received May 19, 2005; revised July 15, 2005.

The authors are with the Centre for Communications Research, University of Bristol, Bristol BS8 1UB, U.K. (e-mail: chris.railton@bristol.ac.uk; d.l.paul@bristol.ac.uk; ian.craddock@bristol.ac.uk; geoff.hilton@bristol.ac.uk).

Digital Object Identifier 10.1109/TAP.2005.860008

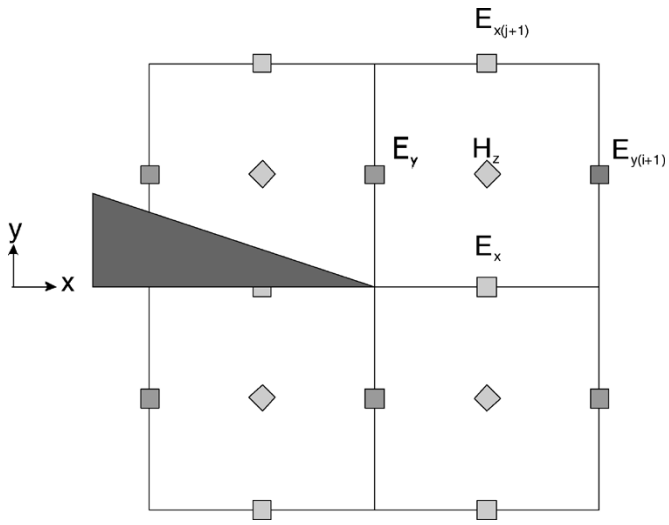

Fig. 1. Perfect electric conductor wedge placed in the FDTD mesh.

actual field variation between nodes, this equation can be modified by including *correction factors* for the line and surface integrals as follows:

$$\mu\delta x\delta y CFM_z \frac{\partial H_z}{\partial t} = E_{x,j+1}\delta x CLE_{x,j+1} + E_{y,i}\delta y CLE_{y,i} - E_{x,j}\delta x CLE_{x,j} - E_{y,i+1}\delta y CLE_{y,i+1} \quad (3)$$

where CFM and CLE are factors which relate the integrals of the known asymptotic field variation to the integrals calculated using the linear approximation. The field values are those at the position of the corresponding node point. This approach is used in [4] and [5] for the two-dimensional (2-D) case and where the edge of the strip coincides with the edges of the FDTD cells. A similar approach is used in [6] to model a coplanar line and is extended in [7] to the analysis of a three-dimensional (3-D) coplanar open stub, including the effects of a right angle bend.

In [8], although the same basic method is applied to 2-D problems, extra terms of the field expansion (1) are retained in order to yield a higher order approximation. The coefficients of the expansion must now be calculated from the field values at several different nodes. This has been shown to provide good results for the cutoff frequencies of a finline even when the edge is placed arbitrarily within the FDTD mesh. However, the algorithm is a complicated one which requires much care to obtain the parameters accurately.

A higher order approximation to the field expansion, consisting of the first two terms in the series (1) is applied in [9] to the full 3-D problems of a patch antenna and a waveguide iris. Good results are reported for these example structures.

The same starting point of the series (1) is used in [10] to derive correction factors which have the same form as MAMPs and which are applied to the example of shielded stripline. However, in [10], MAMPs are only derived for the radial E field component in the plane of the strip and for the case where the edge of the strip coincides with the edge of the FDTD cells. Also, the value taken for the MAMP is obtained semi-empirically by using the value which yields the most accurate result for characteristic impedance over a range of cell sizes. In this contribution, it is shown that similar accuracy is obtained when the analytical MAMPs are used directly.

In [11], the method is applied to more complicated situation of diagonal strips. The update equations which are derived also have the same structure as (3).

In [12], the derivation is done in a different way in that the correction factors are derived in two stages. Firstly, the singular nature of the radial electric and circulating magnetic field components are taken into account and then the effect caused by the use of a Cartesian mesh in the presence of a circular symmetric field is included. Again the form of the update equations is the same as that of (3).

In general, the values of CLE used in (3) may all be different from each other. This means that the model does not necessarily correspond to any physical material and, therefore, reciprocity and local charge conservation may be difficult, or impossible, to enforce. A key property which is fundamental to the method described in this contribution is that, as explained in Section III, $CLE_{x,j} = CLE_{x,j+1} = CLE_{y,i} = CLE_{y,i+1}$ and $CFM_z = 1$. Thus (3) can be rewritten in a simpler form as

$$\mu\mu_z\delta x\delta y\frac{\partial H_z}{\partial t} = E_{x,j+1}\delta x + E_{y,i}\delta y - E_{x,j}\delta x - E_{y,i+1}\delta y. \quad (4)$$

Here, μ_z is a single correction factor which takes the form of a modification to the permeability of the material within the cell. Thus reciprocity and conservation of charge is guaranteed and stability issues are more easily addressed.

III. Analytical Derivation of MAMPs

Consider Maxwell's equations in integral form

$$\frac{\partial}{\partial t}\iint_S \varepsilon E\cdot dS = \oint H\cdot dl \quad (5)$$

$$\frac{\partial}{\partial t}\iint_S \mu H\cdot dS = -\oint E\cdot dl. \quad (6)$$

Applying these to an FDTD mesh in the usual way yields

$$\begin{aligned}\delta y\delta z\frac{\partial}{\partial t}\langle\langle E_x(i+0.5,j,k)\rangle\rangle_{yz} &= \frac{1}{\varepsilon}\Big(\delta y\Big(\langle H_y(i+0.5,j,k-0.5)\rangle_y \\ &\quad - \langle H_y(i+0.5,j,k+0.5)\rangle_y\Big) \\ &\quad - \delta z\left(\langle H_z(i+0.5,j-0.5,k)\rangle_z\right. \\ &\quad \left. - \langle H_z(i+0.5,j+0.5,k)\rangle_z\right)\Big) \quad (7)\end{aligned}$$

$$\begin{aligned}\delta y\delta z\frac{\partial}{\partial t}\langle\langle H_x(i,j+0.5,k+0.5)\rangle\rangle_{yz} &= \frac{1}{\mu}\Big(\delta y\Big(\langle E_y(i,j+0.5,k+1)\rangle_y \\ &\quad - \langle E_y(i,j+0.5,k)\rangle_y\Big) \\ &\quad - \delta z\left(\langle E_z(i,j+1,k+0.5)\rangle_z\right. \\ &\quad \left. - \langle E_z(i,j,k+0.5)\rangle_z\right)\Big) \quad (8)\end{aligned}$$

where δx, δy and δz are the cell sizes $i, j,$ and k are the serial numbers of the cell, $\langle a\rangle_x$ is the average of the quantity, a, along an x directed cell edge and $\langle\langle a\rangle\rangle_{xy}$ is the average of the quantity,

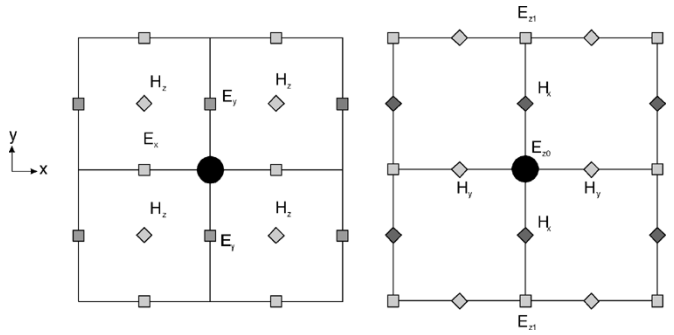

Fig. 2. Thin wire embedded in the FDTD mesh. (left) TE plane and (right) TM plane.

a, over an xy cell face. The other four update equations can be obtained by rotating the coordinates. This approach is similar to that used in the finite integration technique, [13], [14].

In order to complete this set of equations it is necessary to relate the surface averages on the left hand sides to the line averages on the right hand sides. If the fields are assumed to be constant within each cell, which is equivalent to expanding them in a set of pulse basis functions, then the two are the same and the standard FDTD update equations are obtained. However, in the vicinity of a wire or an edge, if the asymptotic field behavior is known, a more accurate relation can be obtained.

Inspection of the equations shows that the ratios of the surface averages to the line averages can be expressed as a modification to the material parameters in the cell. This leads to a particularly simple and physically meaningful result. For example

$$\begin{aligned}\frac{\partial}{\partial t}&\langle E_x(i+0.5,j,k)\rangle_x \\ &= \frac{1}{\varepsilon\varepsilon_x\delta y\delta z}\Big(\delta y\Big(\langle H_y(i+0.5,j,k-0.5)\rangle_y \\ &\qquad - \langle H_y(i+0.5,j,k+0.5)\rangle_y\Big) \\ &\quad - \delta z\left(\langle H_z(i+0.5,j-0.5,k)\rangle_z\right. \\ &\qquad \left. - \langle H_z(i+0.5,j+0.5,k)\rangle_z\right)\Big) \quad (9)\end{aligned}$$

where

$$\varepsilon_x = \frac{\langle\langle E_x\rangle\rangle_{yz}}{\langle E_x\rangle_x}. \quad (10)$$

As long as the behavior of the x component of the E field is known in the space surrounding the singularity, this parameter is readily calculated. In the final program, only the line integrals are stored, the surface integrals are not explicitly calculated.

A. Application to Wires

Consider the case of a thin wire located along a line of E_z nodes as shown in Fig. 2.

The asymptotic field behavior is well known and given as follows:

$$E_x(x,y) \propto H_y(x,y) \propto \frac{x}{x^2+y^2} \quad (11)$$

$$E_y(x,y) \propto H_x(x,y) \propto \frac{y}{x^2+y^2} \quad (12)$$

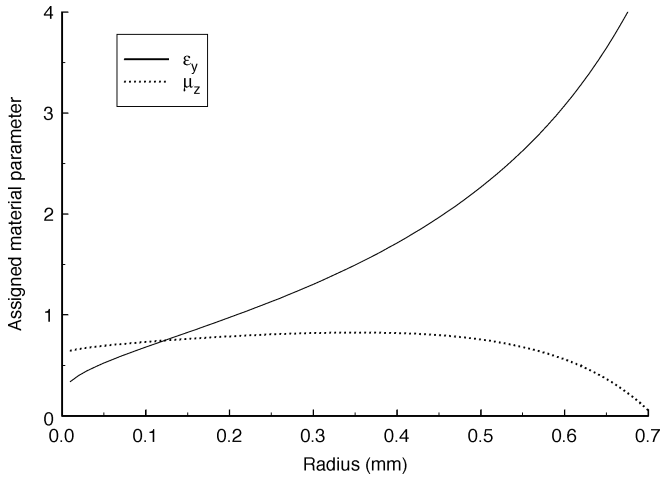

Fig. 3. Required assigned material parameters for a thin wire. $dx = dy = 1$ mm.

$$E_z(x,y) \propto H_z(x,y) \propto Ln\left(\frac{\sqrt{x^2+y^2}}{a}\right) \quad (13)$$

where a is the wire radius.

The required ratios which yield the MAMPs follow immediately:

$$\begin{aligned}\mu_y &= \frac{\langle E_x\rangle_x}{\langle\langle E_x\rangle\rangle_{yz}} = \frac{\langle\langle H_y\rangle\rangle_{xz}}{\langle H_y\rangle_y} = \frac{\delta y\int_a^{\frac{\delta x}{2}}\frac{x}{x^2+y^2}dx}{\delta x\int_{-\frac{\delta y}{2}}^{\frac{\delta y}{2}}\frac{x}{x^2+y^2}dy} \\ &= \frac{\ln\left(\frac{\delta x}{a}\right)}{2\tan^{-1}\left(\frac{\delta y}{\delta x}\right)}\frac{\delta y}{\delta x} \quad (14)\end{aligned}$$

$$\begin{aligned}\mu_x &= \frac{\langle E_y\rangle_y}{\langle\langle E_y\rangle\rangle_{xz}} = \frac{\langle\langle H_x\rangle\rangle_{yz}}{\langle H_x\rangle_x} = \frac{\delta x\int_a^{\frac{\delta y}{2}}\frac{y}{x^2+y^2}dy}{\delta y\int_{-\frac{\delta x}{2}}^{\frac{\delta x}{2}}\frac{y}{x^2+y^2}dx} \\ &= \frac{\ln\left(\frac{\delta y}{a}\right)}{2\tan^{-1}\left(\frac{\delta x}{\delta y}\right)}\frac{\delta x}{\delta y} \quad (15)\end{aligned}$$

$$\mu_z = \frac{\langle\langle H_z\rangle\rangle_{xy}}{\langle H_z\rangle_z} = \frac{2\int_0^{\frac{\pi}{4}}\int_a^{\frac{1}{\cos(\theta)}}\ln\left(\frac{r}{a}\right)drd\theta}{\ln\left(\frac{\sqrt{\left(\frac{\delta x}{2}\right)^2+\left(\frac{\delta y}{2}\right)^2}}{a}\right)}\frac{\delta z}{\delta x\delta y}. \quad (16)$$

In Fig. 3, the required material parameters μ_z and ε_y are shown as a function of wire radius for a cell size of 1 mm. By symmetry, $\mu_x = 1/\varepsilon_y$, which in turn indicates that the velocity of a z directed wave is unaffected by this modification.

It is found that the parameter for H_z, μ_z, is fairly constant so long as the wire radius is less than half the cell size but that it becomes very small as the radius approaches the cell size. Such small values could lead to stability problems although, for radii less than half the cell size, no penalty in time step was encountered. In practice, however, it has been found that altering μ_z has little effect on the observed results and this parameter is therefore left unmodified.

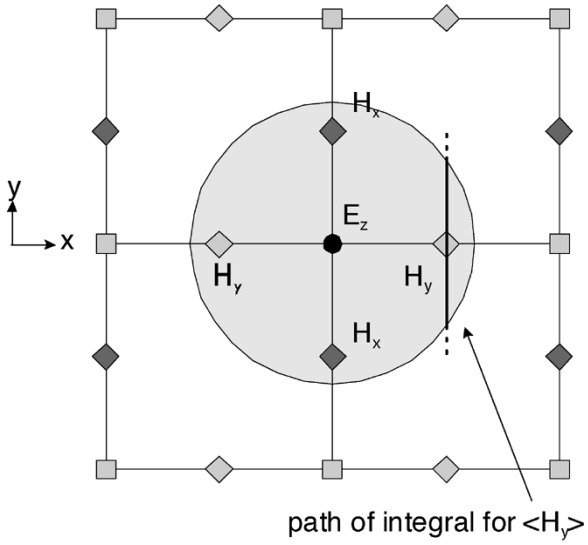

Fig. 4. Theoretical and actual integral paths for calculating $\langle \mathrm{H}_y \rangle$.

For the case where the wire radius is greater than half the cell size, the integration limits should theoretically be altered to account for the fact that the field is zero inside the wire. For instance, μ_x, would be evaluated as follows:

$$\mu_x = \frac{\delta x \int_{a}^{\frac{\delta y}{2}} \frac{y}{x^2+y^2} dy}{2\delta y \int_{\sqrt{a^2-\left(\frac{\delta x}{2}\right)^2}}^{\frac{\delta x}{2}} \frac{y}{x^2+y^2} dx} \frac{\delta x}{\delta y}. \tag{17}$$

It has been found in practice, however, that results obtained in this way are unrealistic and lead to inaccurate results. On the other hand, accurate results are obtained if the MAMPs are calculated using (14) and (15) with the limits unaltered. This situation is shown in Fig. 4 where the dashed lines show the location of the theoretical integral path, since the field inside the wire, shown as a grey circle, is zero. The actual integral is taken over the complete line, including the solid section. If this procedure is done, then the required values of μ_x and μ_y are well behaved even though they do become large when the radius of the wire approaches the cell size. As will be seen later, consistently good results can be obtained with wires having a radius considerably larger than half the size of the cell.

It can be shown that, for wire radii less than half the cell size, the update equations obtained using this method are formally identical to those used in [12] although they are obtained more directly here. The method of [12] is, however, limited to wires less than half the cell size in radius.

It has been found that, in the geometries tested, a time step of 0.95C for wires of radius greater than 15% of the cell size and a time step of 0.886C for wires of radius greater than 5% of the cell size, where C is the Courant limit for unmodified FDTD, gave stable behavior even if the run was continued for 64 000 iterations.

B. Application to Narrow Strips

The fields in the vicinity of a thin strip orientated in the z direction, lying on the xz plane and at a height h, above a ground plane can be expressed as follows [15]:

$$\begin{aligned} E_x(x,y) &\propto H_y(x,y) \\ &\propto \mathrm{Im}\left(\sqrt{\frac{w}{(y+ix)^2+\left(\frac{w}{2}\right)^2}} - \sqrt{\frac{w}{(y+2h+ix)^2+\left(\frac{w}{2}\right)^2}} \right) \end{aligned} \tag{18}$$

$$\begin{aligned} H_x(x,y) &\propto E_y(x,y) \\ &\propto \mathrm{Re}\left(\sqrt{\frac{w}{(y+ix)^2+\left(\frac{w}{2}\right)^2}} + \sqrt{\frac{w}{(y+2h+ix)^2+\left(\frac{w}{2}\right)^2}} \right). \end{aligned} \tag{19}$$

See (20) and (21) at the bottom of the page. The required MAMPs are therefore given as follows:

$$\begin{aligned} \mu_y &= \frac{\langle E_x \rangle_x}{\langle\langle E_x \rangle\rangle_{yz}} = \frac{\langle\langle H_y \rangle\rangle_{xz}}{\langle H_y \rangle_y} \\ &= \frac{\delta y \int_{\frac{w}{2}-(\beta-1)\delta x}^{\frac{w}{2}-\beta\delta x} Hy(x,0)dx}{\delta x \int_{-\frac{\delta y}{2}}^{\frac{\delta y}{2}} Hy\left(\frac{w}{2}-(\beta-0.5)\delta x, y\right) dy} \end{aligned} \tag{22}$$

$$\begin{aligned} E_z(x,y) &\propto \int H_y dx \propto \int E_y dy \\ &= \mathrm{Re}\left(\sqrt{w} \ln\left(\frac{\frac{w}{2}}{y+ix+\sqrt{(y+ix)^2+\left(\frac{w}{2}\right)^2}} \right) - \sqrt{w} \ln\left(\frac{\frac{w}{2}}{y+2h+ix+\sqrt{(y+2h+ix)^2+\left(\frac{w}{2}\right)^2}} \right) \right) \end{aligned} \tag{20}$$

$$\begin{aligned} H_z(x,y) &\propto \int E_y dx \propto \int H_y dy \\ &\propto \mathrm{Im}\left(\sqrt{w} \ln\left(\frac{\frac{w}{2}}{y+ix+\sqrt{(y+ix)^2+\left(\frac{w}{2}\right)^2}} \right) + \sqrt{w} \ln\left(\frac{\frac{w}{2}}{y+2h+ix+\sqrt{(y+2h+ix)^2+\left(\frac{w}{2}\right)^2}} \right) \right) \end{aligned} \tag{21}$$

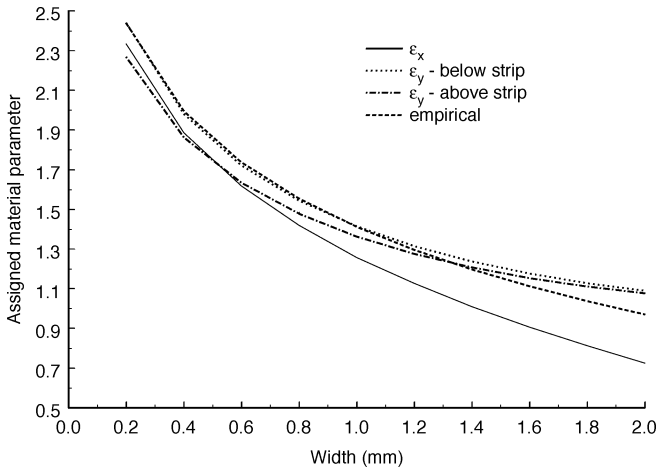

Fig. 5. Required assigned material parameters for a strip. $dx = dy = 2$ mm.

$$\mu_x = \frac{\langle E_y \rangle_y}{\langle\langle E_y \rangle\rangle_{xz}} = \frac{\langle\langle H_x \rangle\rangle_{yz}}{\langle H_x \rangle_x} = \frac{\delta x \int_0^{\delta y} Ey\left(\frac{w}{2} - \beta\delta x, y\right) dy}{\delta y \int_{\frac{w}{2}-(\delta+0.5)\delta x}^{\frac{w}{2}-(\beta-0.5)\delta x} Ey\left(x, \frac{\delta y}{2}\right) dx} \tag{23}$$

where $\beta\delta x$ is the distance of the strip edge from the cell boundary.

In Fig. 5 the calculated MAMPs for a strip height of 10 mm and a cell size of 2 mm are shown. Here it is shown that the values are well behaved for all strip widths less than the cell size. For widths between one cell size and two cell sizes it has not been possible to apply this method directly. The values obtained using the empirical approach of [1] are shown for comparison. In that situation, ε_x and ε_y take the same value and this can be seen to lie close to the analytical value of ε_y.

It has been found that, in the geometries tested, a time step of 0.95C for strips of width greater than 30% of the cell size, 0.886C for strips of radius greater than 10% of the cell size and 0.7C for strips of width greater than 2.5% of cell size, where C is the Courant limit for unmodified FDTD, gave stable behavior even if the run was continued for 64 000 iterations.

C. Application to Wide Strips and Patches

The method described in Section III-B is readily applicable to the case where the width of the strip is greater than the size of the cell. In this case the affected cells are the ones which contain the edges. In Fig. 6, the marked E_x, E_y, H_x, and H_y nodes are modified using the values derived from (22) and (23) where βdx is the distance by which the edge protrudes into the cell.

IV. Results Obtained Using Analytically Derived MAMPs

A. Wire Transmission Line

Transmission lines consisting of a wire above a ground plane were considered as the first examples. For this test, three different heights 8, 10, and 20 mm, were used. The cell size was 2 mm and radii of between 0.05 and 1.6 mm were considered. The

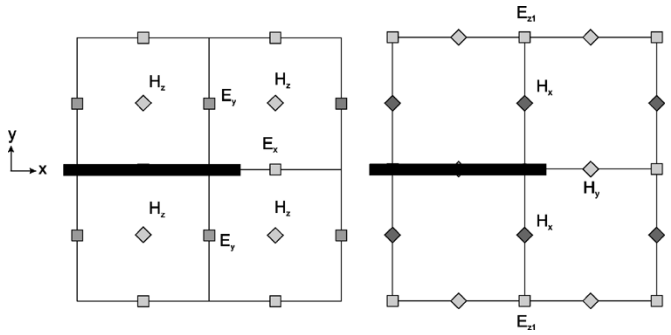

Fig. 6. Wide strip or patch embedded in the FDTD mesh. (left) TE plane and (right) TM plane.

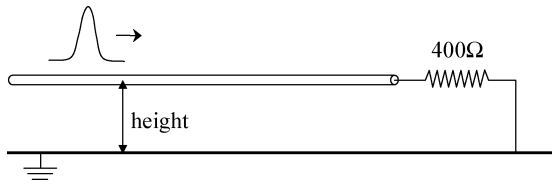

Fig. 7. Geometry of the wire transmission line.

wire was terminated at the end by a 400 Ω resistor as indicated in Fig. 7. A raised cosine pulse was launched along the wire.

The impedance was calculated in two different ways. First, the amplitude of this incident pulse was compared with the amplitude of the pulse reflected from the resistor. Secondly, a snapshot of the field distribution around the wire was taken as the pulse went past and the voltages and currents in the strip were calculated from these field values. It is noted that, because the line integrals of the field components are stored, rather than the amplitude at the node position, no further account need be taken of the singular behavior of the field at this stage. By obtaining consistent results from these two methods, confidence is gained not only that the singular fields are correctly being taken into account but that the discontinuity between the wire and the resistor is also being correctly handled. The structure is the same as is used in [16] and [17].

The results are shown in Figs. 8 and 9 where it can be seen that the two methods of calculating the impedance do give very similar results. It can be seen that, in each case, the calculated impedance is somewhat over-estimated but, nevertheless, is within 2.5% of analytical results for heights of 8 and 10 mm and within 5% for the height of 20 mm. In addition, it can be seen that, in contrast to some other methods, eg., [12] and [18], the agreement remains good even when the wire radius is greater than half a cell size, ie. greater than 1 mm.

B. Shielded Stripline

A shielded stripline structure, having the same geometry as that given in [10], was modeled using the MAMP method in order to compare results. The strip has a width of 2 mm and is centrally placed in a metal box having a cross-section of 8 mm × 4 mm. Calculations of the characteristic impedance of the structure were made using cell sizes of 1, 0.5, and 0.25 mm. The calculated results were compared to the value of 98.922 Ω obtained using a very fine mesh and are shown in Table I. The

TABLE I
RESULTS FOR SHIELDED STRIPLINE

	This research			[10]		
Cell size	ε_x	ε_y	**% error**	ε_x	ε_y	**% error**
1mm	0.594	0.736	0.5	0.66	1.0	0.37
0.5mm	0.633	0.719	0.05	0.66	1.0	0.24
0.25mm	0.667	0.715	0.02	0.66	1.0	0.12

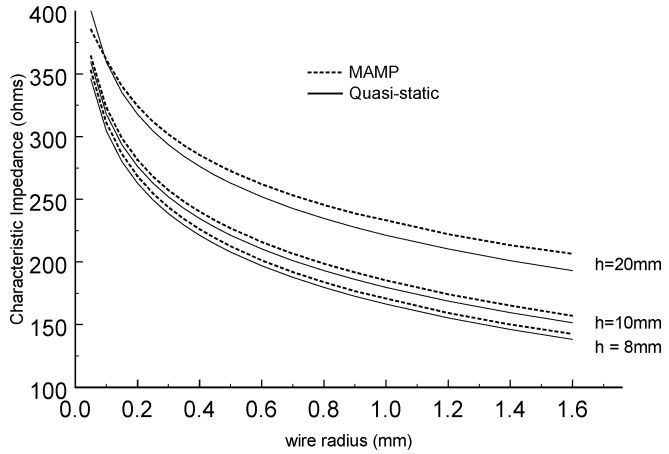

Fig. 8. Characteristic impedance of wire transmission lines calculated from the reflected pulse.

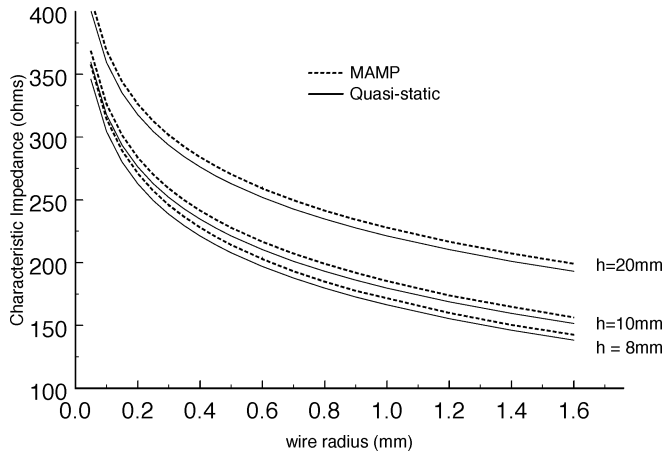

Fig. 9. Characteristic impedance of wire transmission lines calculated from the field snapshot.

table also shows the values for the MAMPs used in this method compared with those used in [10].

It can be seen from these results that, although the error is slightly greater than in [10] for the coarsest mesh, the results are more accurate for the other two meshes tested.

C. Microstrip Transmission Line

In order to demonstrate the technique for microstrip, two different test structures were used. In the first case, a square mesh of size 2 mm and a height of 10 mm was used, in the same way as for the wire transmission line. In the second case, a rectangular mesh of size 1 mm $\times$ 0.3175 mm was used and the strip was placed at heights of 0.635 and 1.27 mm above the ground plane, corresponding to 2 and 4 cells, respectively. In each case results

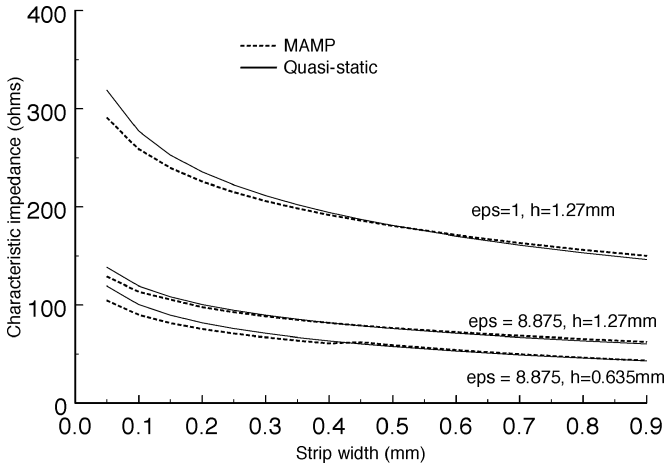

Fig. 10. Calculated characteristic impedance of microstrip. $dy = 0.3175$ mm, $dx = 1$ mm.

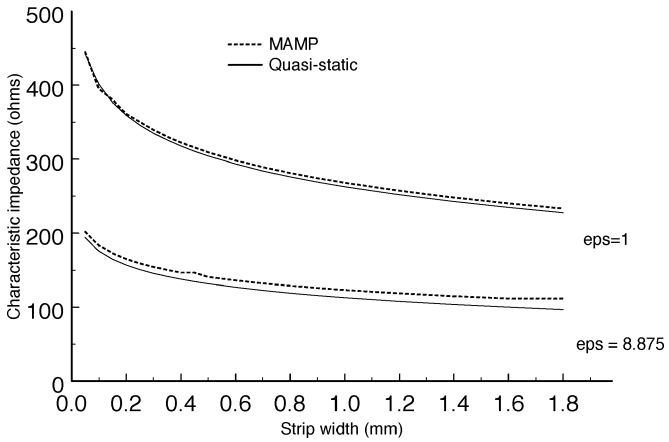

Fig. 11. Calculated characteristic impedance of microstrip. $dy = 2$ mm, $dx = 2$ mm, $h = 10$ mm.

were obtained for substrate dielectric constants of 1 and 8.875. Characteristic impedances were calculated in the same way as for the wire transmission line using the configuration shown in Fig. 7.

The calculated results, compared with a quasistatic formula [19] are shown in Figs. 10 and 11. It can be seen that the agreement is generally very good with a worst case discrepancy of 9% in the case of very small radii.

D. Microstrip Patch Antenna

A microstrip patch antenna, having the dimensions the same as in [9] was modeled using basic FDTD with a coarse, medium and fine mesh and the results compared with those obtained

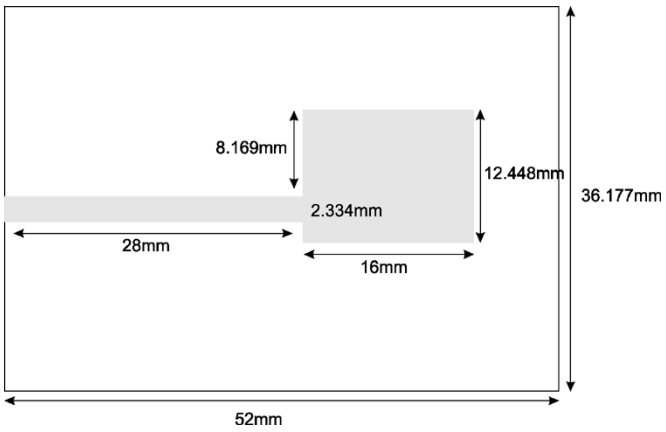

Fig. 12. Plan view of patch antenna.

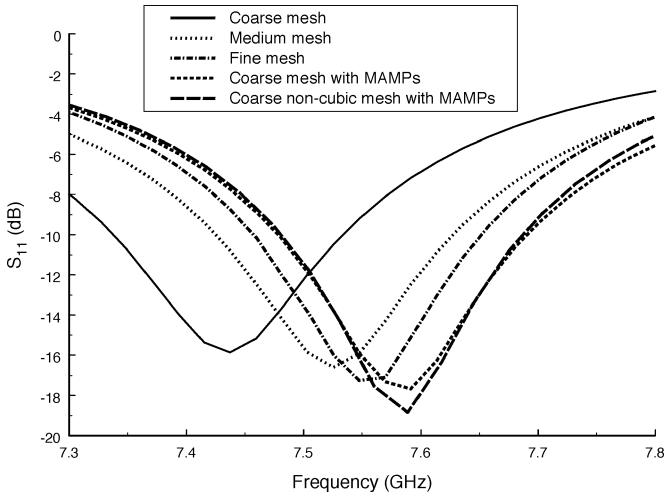

Fig. 13. Calculated results for the return loss of the patch antenna using different mesh sizes.

by using the coarse mesh in conjunction with MAMPs. The geometry of the antenna is shown in Fig. 12. The substrate height was 0.794 mm, the dielectric constant was 2.2 and the box height was 3.97 mm. For the coarse mesh the cell size was $0.389\ \mathrm{mm} \times 0.397\ \mathrm{mm} \times 0.4\ \mathrm{mm}$, for the medium mesh the cell size was $0.1945\ \mathrm{mm} \times 0.1985\ \mathrm{mm} \times 0.2\ \mathrm{mm}$ while for the fine mesh the cell size was $0.097\,25\ \mathrm{mm} \times 0.099\,125\ \mathrm{mm} \times 0.1\ \mathrm{mm}$. These were chosen to be as cubic as possible given the constraints of the geometry. In addition, results were calculated using MAMPs in conjunction with the noncubic coarse mesh used in [9] having a cell size $0.389\ \mathrm{mm} \times 0.1985\ \mathrm{mm} \times 0.4\ \mathrm{mm}$.

The excitation plane and the probe were placed in the same position along the feed line as in [9]. Results for the return loss are given in Fig. 13. It can be seen that the resonant frequencies, calculated using basic FDTD, are converging to approximately 7.6 GHz as the mesh size is reduced. Results obtained using the coarse mesh, enhanced by MAMPs, show good agreement with the converged results for both the cubic and the noncubic meshes.

V. Conclusion

In this contribution it has been shown that wires and strips may be accurately treated in the FDTD method by means of analytically calculated Modified Assigned Material Parameters. This approach has advantages of simplicity, robustness and versatility over other methods of treating geometrical detail while giving equivalent accuracy. The analytic approach to the calculation of MAMPs much reduces the need for empirical look-up tables to be generated and adds rigour.

The technique lends itself to other situations such as strips with finite thickness and finite conductivity. It is robust in that the modified materials are physically realistic and that there is a clear interpretation of the field values assigned to the modified nodes. Boundaries between different objects, such as a microstrip step discontinuity, can be dealt with in a natural and simple manner.

References

[1] C. J. Railton, "The inclusion of fringing capacitance and inductance in FDTD for the robust accurate treatment of material discontinuities," *IEEE Trans. Microw. Theory Tech.*, vol. 48, no. 1, pp. 2283–2288, Jan. 2000.

[2] ——, "The choice of cell size and the use of pre-calculated correction factors in the analysis of planar circuits using FDTD and TLM," in *Proc. Eur. Microwave Conf.*, London, U.K., Sep. 2001, pp. 137–140.

[3] C. J. Railton and D. L. Paul, "Analysis of circular waveguide filter using enhanced FDTD," *Int. J. Numerical Modeling: Electronic Networks, Devices and Fields*, vol. 15, no. 5–6, pp. 535–547, Sep.–Dec. 2002.

[4] G. Mur, "The modeling of singularities in the finite-difference approximations of the time-domain electromagnetic-field equations," *IEEE Trans. Microw. Theory Tech.*, vol. MTT-29, no. 10, pp. 1073–1077, Oct. 1981.

[5] J. Van Hese and D. De Zutter, "Modeling of discontinuities in general coaxial waveguide structures by the FDTD method," *IEEE Trans. Microw. Theory Tech.*, vol. MTT-40, no. 3, pp. 547–556, Mar. 1992.

[6] K. Beilenhoff and W. Heinrich, "Treatment of field singularities in the finite-difference approximation," in *IEEE MTT-S Int. Microwave Symp. Dig.*, 1993, pp. 979–982.

[7] N.-H. Huynh and W. Heinrich, "FDTD accuracy improvement by incorporation of 3D edge singularities," in *IEEE MTT-S Int. Microwave Symp. Dig.*, 1999, pp. 1573–1576.

[8] P. Przybyszewski and M. Mrozowski, "A conductive wedge in Yee's mesh," *IEEE Microw. Guided Wave Lett.*, vol. 8, no. 2, pp. 66–68, Feb. 1998.

[9] T. Kashiwa, M. Uchiya, K. Suzuki, and Y. Kanai, "FDTD analysis of microwave circuits using edge condition," *IEEE Trans. Magn.*, vol. 38, no. 2, pp. 705–708, March 2002.

[10] M. Celuch-Marcysiak, "Local stereoscopic field singularity models for FDTD analysis of guided wave problems," in *IEEE MTT-S Int. Microwave Symp. Dig.*, 2003, pp. 1137–1140.

[11] S. M. Foroughipour and K. P. Esselle, "The theory of singularity-enhanced FDTD method for diagonal metal edges," *IEEE Trans. Antennas Propag.*, vol. 51, no. 2, pp. 312–321, Feb. 2003.

[12] R. M. Makinen, J. S. Juntunen, and M. A. Kivikoski, "An improved thin wire model for FDTD," *IEEE Trans. Microw. Theory Tech.*, vol. 50, pp. 1245–1255, May 2002.

[13] T. Weiland, "A discretization method for the solution of Maxwell's equations for six component fields," *Electronics and Communication (AEU)*, vol. 31, pp. 116–120, 1977.

[14] ——, "Time domain electromagnetic field computation with finite difference methods," *Int. J. Numerical Modeling: Electronic Networks, Devices and Fields*, vol. 9, pp. 259–319, 1996.

[15] I. J. Craddock and C. J. Railton, "A new technique for the stable incorporation of static field solutions in the FDTD method for the analysis of thin wires and narrow strips," *IEEE Trans. Microw. Theory Tech.*, vol. MTT-46, no. 8, pp. 1091–1096, Aug. 1998.

[16] B. P. Koh, C. J. Railton, and I. J. Craddock, "Wire above ground plane transmission line formulation in the FDTD algorithm," *Proc. Inst. Elect. Eng. Microwaves, Antennas and Propagation*, vol. 151, no. 3, pp. 249–255, Jun. 2004.

[17] C. J. Railton, B. P. Koh, and I. J. Craddock, "The treatment of thin wires in the FDTD method using a weighted residuals approach," *IEEE Trans Antennas Propag.*, vol. 52, no. 11, pp. 2941–2949, Nov. 2004.

[18] K. Umashankar and A. Taflove, "Calculation and experimental validation of induced currents on coupled wires in an arbitrary shaped cavity," *IEEE Trans. Antennas Propag.*, vol. AP-35, pp. 1248–1257, 1987.
[19] C. A. Balanis, *Advanced Engineering Electromagnetics*. New York: Wiley.

Chris J. Railton received the B.Sc. degree in physics with electronics from the University of London, London, U.K., in 1974 and the Ph.D. degree in electronic engineering from the University of Bath, Bath, U.K., in 1988.

During 1974 to 1984, he worked in the Scientific Civil Service on a number or research and development projects in the areas of communications, signal processing and EMC. Between 1984 and 1987, he worked at the University of Bath on the mathematical modeling of boxed microstrip circuits. He currently works in the Centre for Communications Research, University of Bristol, Bristol, U.K., where he leads the Computational Electromagnetics group which is engaged in the development of new algorithms for electromagnetic analysis and their application to the design of MMIs, planar and conformal antennas, microwave and RF heating systems, EMC, high-speed interconnects, and optical waveguide components.

Dominique L. Paul received the D.E.A. degree in electronics from Brest University, Brest, France, in June 1986 and the Ph.D. degree from Ecole Nationale Superieure des Telecommunications de Bretagne (LEST-ENSTBr), France, in January 1990.

From 1990 to 1994, she was a Research Associate at the Centre for Communications Research, University of Bristol, Briston, U.K. During 1994 1996, she worked as a Research Associate at the Escuela Tecnica Superior de Ingenieros de Telecomunicacion, Madrid, Spain under a grant from the Spanish Government. Since 1997, she has been a Research Fellow in the Centre for Communications Research, University of Bristol. Her research interests include the electromagnetic modeling of passive devices such as microwave heating systems, dielectric structures at millimeter wavelengths, low profile antennas and conformal antenna arrays.

Ian J. Craddock received the B.Eng. and Ph.D. degrees from the University of Bristol, Bristol, U.K., in 1992 and 1995, respectively.

He is a Reader in the Centre for Communications Research (CCR), University of Bristol, U.K. He has active research interests in FDTD, wide-band antenna design, antenna arrays, MIMO, electromagnetic analysis and microwave radar for breast cancer detection. He is part of the EU Framework 6 Antennas Network of Excellence, where he leads a work-package on antennas for GPR.

Geoffrey S. Hilton received the B.Sc. degree from the University of Leeds, Leeds, U.K., in 1984 and the Ph.D. degree from the Department of Electrical and Electronic Engineering at the University of Bristol, Briston, U.K., in 1992.

From 1984 to 1986, he worked as a Design Engineer at GEC-Marconi, before commencing research on microwave antennas, first as a Postgraduate and later as a Member of Research Staff, at the University of Bristol. The work included design and analysis of printed antenna elements and arrays, and involved the development of FDTD models for these structures and comparison with measured data. In 1993, he joined the academic staff, lecturing in microwave antennas and satellite communications. Current research interests include radiation pattern synthesis and array modeling, synthetic focusing ground penetrating radar and the design of electrically small antennas and active antennas for mobile communications applications.